Journal of Applied Geophysics 177 (2020) 104040

Contents lists available at ScienceDirect

Journal of Applied Geophysics

journal homepage: www.elsevier.com/locate/jappgeo

Non-remote reference noise cancellation - using reference data in the presence of surface-NMR signals

Mike Müller-Petke *

Leibniz Institute for Applied Geophysics, Stilleweg 2, Hannover D-30655, Germany

ARTICLE INFO

Article history:
Received 15 July 2019
Received in revised form 20 January 2020
Accepted 22 April 2020
Available online 5 May 2020

ABSTRACT

Surface-NMR measurements commonly suffer from low signal-to-noise ratios. In recent years, with the introduction of multi-channel surface-NMR instruments, the technique of remote-reference noise cancellation (RNC) was developed and significantly improved the applicability of surface-NMR. The current formulation of RNC requires a reference loop to be placed a remote distance from the transmitter loop such that no NMR signal is recorded. Reference loops placed at non-remote distances have been envisaged to provide both improved noise cancellation performance and field efficiency; however, the concept has not been previously applied because the theoretical framework was missing. In this paper, the theoretical framework is presented. It is demonstrated that reference loops placed at non-remote distances provide superior noise cancellation performance. Considerations for placing the reference loop relative to the transmitter loop are provided, and the theoretical framework is evaluated based on a semi-synthetic example using real field noise and synthetic surface-NMR data.

1. Introduction

The surface nuclear magnetic resonance (surface-NMR) method has shown continuous progress and significant improvements in many fields of research from forward modeling (Lehmann-Horn et al., 2011; Grombacher et al., 2019) to inversion (Hertrich et al., 2009; Mueller-Petke and Yaramanci, 2010; Behroozmand et al., 2012; Jiang et al., 2018; Skibbe et al., 2018) and field layouts (Jiang et al., 2015; Costabel et al., 2016; Altobelli et al., 2019) in recent years. Many of these improvements extended the range of applications, mostly with respect to hydrogeological tasks, due to the unique direct sensitivity of surface-NMR to the hydrogen proton and therefore water.

Despite all of these very encouraging developments, the low signal-to-noise ratio (SNR) of the detected signals is still a key problem that limits the broad application of surface-NMR. The measured surface-NMR signals are typically within the range of a few hundred nanovolts and can be significantly contaminated by electromagnetic noise. Therefore, improving the SNR is a necessary development and a very active field of research. The very first attempts to improve the SNR were based on a figure-eight loop design (Trushkin et al., 1994). This layout can effectively cancel noise but is limited to a single noise source, thus doubling the required size of a single loop to reach the same depth of investigation and flat terrain. Further developments in the field of enhancing the SNR generally cover (i) advanced pulse experiments (e.g., Grunewald et al., 2016) to increase the signal amplitude, (ii) advanced signal processing techniques (Larsen et al., 2014; Wang et al., 2018; Liu et al., 2019; Lin et al., 2019) and (iii) reference measurements to reduce the amplitude of the environmental electromagnetic noise (Walsh, 2008; Dalgaard et al., 2012).

While signal processing techniques aim to identify and separate the surface-NMR signal from electromagnetic noise using data from a single detection channel, the reference approach utilizes additional reference channels without surface-NMR signals to independently characterize the electromagnetic noise. Such techniques have been used since the 1980s in, e.g., magnetotellurics (MT) and transient electromagnetism (TEM) (Gamble et al., 1979). The reference approach became popular with the development of surface-NMR instruments that provided the necessary multi-channel data acquisition system (Radic, 2006; Walsh, 2008). Since then, several methods using a reference loop-based system have been developed. Radic (2006) presented a remote reference approach operating in the frequency domain and using vertical loops of 1 m size as references. (Walsh, 2008) demonstrated an adaptive signal processing algorithm implemented in the Vista-Clara software. An adaptive filter in the time domain was presented by Dalgaard et al. (2012). Müller-Petke and Costabel (2014) compared time- and frequency-domain approaches. All approaches have demonstrated a useful capability to improve the SNR of surface-NMR data. All approaches rely on a reference placed some distance from the surface-NMR transmitter loop, as the reference loop must not detect any

* Corresponding author.
E-mail address: mike.mueller-petke@leibniz-liag.de.

https://doi.org/10.1016/j.jappgeo.2020.104040

surface-NMR signal. However, both the field effort and the performance of the noise cancellation may benefit from the ability to place the reference loop closer to the transmitter loop, i.e., at a not remote distance, as it is expected that the correlation between the environmental noise decreases with decreasing distance between loops.

In this paper, a theoretical framework that allows the reference to be placed close to the transmitter is presented and evaluated. Furthermore, the noise cancellation performance of reference loops as a function of the distance between two loops is investigated. Finally, preliminary research on optimal positioning of a non-remote reference loop is presented.

2. Fundamentals of reference-based noise cancellation

To provide the necessary theoretical background for deriving the framework of non-remote reference noise cancellation, a brief review on remote reference noise cancellation (RNC) based on the formulation in Müller-Petke and Costabel (2014) is given here.

Considering two loops s and r, placed some distance from each other, and recorded environmental electromagnetic field n, we write

$$s = n_{Rx} \tag{1}$$

and

$$r = n_{Nx} \tag{2}$$

with Rx and Nx indicating the different locations in the electromagnetic noise field. Now, a filter h that transforms the signal in s to the one detected by r can be calculated according to

$$rs_t = \sum_{\tau} h_\tau rr_{t-\tau} \tag{3}$$

with rr and rs being the auto-correlation of r and the cross-correlation of r with s, respectively. Eq. (3) describes an optimal (or Wiener) filter that minimizes the mean-squared difference between the transformed signal $\hat{r}$ (calculated as the convolution of h and r) and the target signal s. Müller-Petke and Costabel (2014) refer to h as the transfer function (TF). The TF coefficients can be derived in either the time or frequency domain. As the TF coefficients are based on the cross- and auto-correlations of r and s, the higher the correlation between the two signals is, the lower the mean-squared difference. Subtracting $\hat{r}$ from s leads to a signal $\hat{s}$ that is reduced by correlated noise. The loop providing the signal r is referred to as the reference loop. Obviously, only correlated noise can be canceled. Since correlation is the key in reference-based noise cancellation, one can assume that the closer two loops are placed to each other, the more the signal components are correlated, and thus, the noise-reduced signal $\hat{s}$ is of the lowest remaining amplitude. Even though the data as presented in Fig. 1 cannot be generalized, they indicate that the assumption that RNC results improve when decreasing the distance between the loops is valid for this site. The noise data were recorded at a field site in Hannover, Germany. The site is very close to a city tram line and street traffic (approximately 200 m), a highway (approximately 50 m) and city buildings (approximately 100 m). A large waste disposal site including an energy-from-waste facility is within approximately 1 km distance. The site is impacted by many different noise sources that also change with time.

When conducting surface-NMR experiments, one loop becomes a surface-NMR signal receiver, and the other becomes the reference loop. Considering the distance between the two loops, two cases must be distinguished:

1. The reference loop is remote, meaning that surface-NMR signals cannot be detected.
2. The reference loop is non-remote, meaning that surface-NMR signals are detected.

3. Remote-reference noise cancellation (remote RNC)

In the case of a remotely placed reference loop, only the receiver loop detects surface-NMR signals, and thus, eq. (2) remains unchanged, while the signal detected in s reads

$$s^{NMR} = s_{Rx}^{NMR} + n_{Rx} \tag{4}$$

with s_{Rx}^{NMR} indicating the surface-NMR signal. To improve the data quality in the receiver loop, the TF is applied to the remote-reference signal r, and the resulting signal is subtracted. Thus, the signal $\hat{s}$ reads (in the time domain)

$$\hat{s} = s^{NMR} - \hat{r} \tag{5}$$

$$= s_{Rx}^{NMR} + n_{Rx} - TF \circledast r \tag{6}$$

$$= s_{Rx}^{NMR} + n_{Rx} - TF \circledast n_{Nx} \tag{7}$$

$$= s_{Rx}^{NMR} + n_{UC} \tag{8}$$

with n_{UC} representing the remaining uncorrelated noise. Targeting inverse modeling, the receiver detected surface-NMR signal can be simulated by the receiver kernel function $\mathbf{G_{Rx}}$ and a subsurface model m as

$$s_{Rx}^{NMR} = \mathbf{G_{Rx}} \cdot m \tag{9}$$

4. Non-remote reference noise cancellation (non-remote RNC)

In contrast, a reference loop placed non-remotely detects surface-NMR signals, and eq. (2) becomes

$$r^{NMR} = r_{Nx}^{NMR} + n_{Nx} \tag{10}$$

Thus, both the receiver and the reference include surface-NMR signals. Applying again the TF on the reference loop record r and subtracting the transformed reference signal, we obtain

$$\hat{s} = s^{NMR} - \hat{r}^{NMR} \tag{11}$$

$$= s_{Rx}^{NMR} + n_{Rx} - TF \circledast r^{NMR} \tag{12}$$

$$= s_{Rx}^{NMR} + n_{Rx} - TF \circledast \left(r_{Nx}^{NMR} + n_{Nx}\right) \tag{13}$$

Using the convolution theorem

$$TF \circledast (f + g) = TF \circledast f + TF \circledast g \tag{14}$$

we obtain

$$\hat{s} = s_{Rx}^{NMR} + n_{Rx} - TF \circledast r_{Nx}^{NMR} + TF \circledast n_{Nx} \tag{15}$$

$$= s_{Rx}^{NMR} - TF \circledast r_{Nx}^{NMR} + n_{UC} \tag{16}$$

Compared to the situation in which no surface-NMR signal is present in the reference loop r, the main difference involves handling the application of the TF to the reference loop detected NMR signal r_{Nx}^{NMR}. Again, targeting inverse modeling, we replace the individual surface-NMR signals by their respective model responses, with $\mathbf{G_{Nx}}$ being the kernel function of the reference loop,

$$\hat{s} = \mathbf{G_{Rx}} \cdot m - TF \circledast (\mathbf{G_{Nx}} \cdot m) \tag{17}$$

and finally obtain

$$\hat{s} = [\mathbf{G_{Rx}} - TF \circledast \mathbf{G_{Nx}}] \cdot m \tag{18}$$

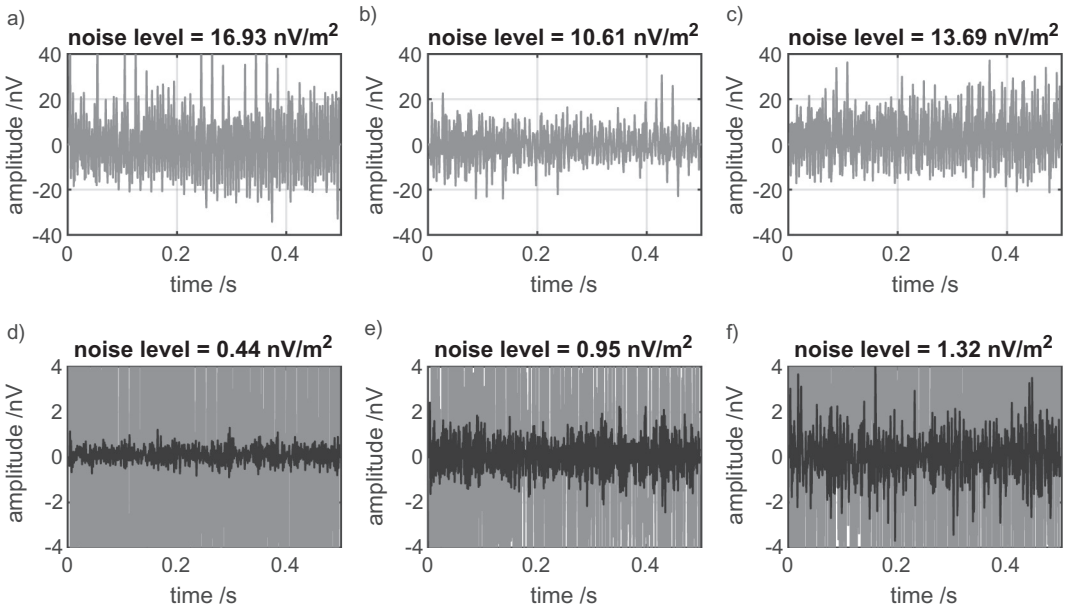

Fig. 1. Reference-based noise cancellation performance as a function of the distance between two loops. Signals are recorded using a 10 m square loop as the detection loop and a 10 m square loop as the reference loop positioned at 10 m (a,d), 30 m (b,e) and 50 m (c,f) from the detection loop. The signals in a), b) and c) are the raw signals (gray lines), while d), e) and f) show the signals after noise cancellation (black lines), with the raw signals shown in gray for comparison. When only two channels are available, three datasets are measured to vary the distance between the two loops. The data were recorded at a field site in Hannover, Germany.

$$= \mathbf{G}_{\mathbf{RNC}} \cdot m \tag{19}$$

Thus, forward modeling of the noise-reduced signal $\hat{s}$ can be carried out by deriving a new kernel function $\mathbf{G}_{\mathbf{RNC}}$ that contains both kernel functions $\mathbf{G}_{\mathbf{Rx}}$ and $\mathbf{G}_{\mathbf{Nx}}$ modified by the TF. The new kernel function $\mathbf{G}_{\mathbf{RNC}}$ is independent of the model and is not updated during the inversion. However, this is true only if a multi-exponential QT-Inversion is used. If a mono-exponential QT-Inversion is used, then the kernel function becomes model dependent (Müller-Petke et al., 2016) and is updated in each iteration to include the TF. As the TF is a constant factor (that is not model dependent), this does not impact the stability of currently applied mono-exponential QT-Inversions.

Note that the kernel function must be modified to simulate the surface-NMR signal oscillating at the Larmor frequency in order to apply the TF. Obviously, if the kernel function is modified to simulate the signal oscillating at the Larmor frequency, then the new kernel function can be Fourier-transformed, and the TF in the frequency domain can be applied. Due to the advantages of calculating the TF in the frequency domain, as shown by Müller-Petke and Costabel (2014), this approach is used in the following. Appendix A provides pseudo-code that provides insight into how a QT-Inversion that includes a non-remote NC can be implemented.

5. Results and discussion

5.1. Positioning a non-remote reference loop

Based on eq. (18), $\mathbf{G}_{\mathbf{Rx}}$ and $\mathbf{G}_{\mathbf{Nx}}$ must not be similar to each other since, in addition to canceling the noise, the NMR signal would also be canceled. It is reasonable to expect that reference positions with associated $\mathbf{G}_{\mathbf{Nx}}$ can be derived that not only prevent cancellation of the NMR signal but also even enhance the signal amplitude. In the following, a preliminary study of positioning of the non-remote reference loop is presented, and some general features are discussed. Common to all layouts is a 50 m one turn diameter circular loop serving as a transmitter and a receiver. The subsurface is set as resistive and fully saturated. The Earth's magnetic field is set to 60° inclination and 48,000 nT.

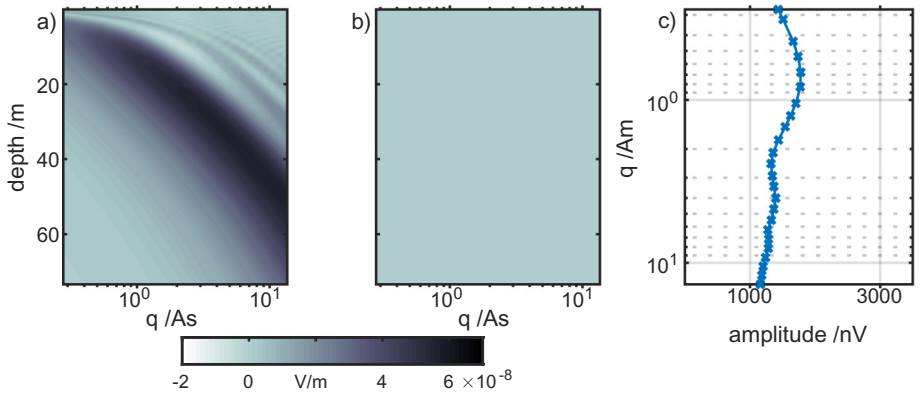

Fig. 2. Real part (a) and imaginary part (b) of a 50 m diameter coincident loop kernel function. The kernel function is calculated for a resistive subsurface with the Earth's magnetic field at 48,000 nT and a 60° inclination. The sounding curve (c) is simulated for a fully saturated homogeneous ground, i.e., representing the maximum detectable signal amplitude.

According to the resistive subsurface, the imaginary part of the kernel function is zero (Fig. 2).

A 10 m diameter multi-turn circular loop is used as reference loop. This loop size can be easily handled under the field conditions. The kernel function of the 10 m loop is calculated similarly to that of a separated loop (Hertrich et al., 2005), i.e., the 50 m diameter loop acts as a transmitter and the 10 m loop as a receiver. To apply eq. (18), the TF must be considered. As the general relationship between the two kernel functions ($\mathbf{G_{Rx}}$ and $\mathbf{G_{Nx}}$) is to be investigated, the 10 m reference loop is set up with 25 turns to achieve a total area equal to that of the 50 m receiver loop, and homogeneous noise conditions are assumed. This leads to $TF = 1$, and the two kernel functions can be simply subtracted.

First, the reference loop is placed in the center of the transmitter loop and 12.5 m and 35 m north of the center (Fig. 3 - red dotted-dashed lines). The imaginary parts of all non-remote reference kernel functions (Fig. 4 b, g, l) are very small, as the ground is set as resistive and the reference loop is placed to the north (see Hertrich et al. (2005) for a general discussion on the imaginary part of the kernel function for separated loops). Therefore, the imaginary part of the non-remote reference does not add any additional signal when subtracted from the coincident loop signal. The real parts of the kernel functions of both in-loop configurations, i.e., the centered and 12.5 m shifted configurations, show similar sensitivity patterns compared to the coincident loop (Fig. 2a), i.e., the main sensitivity increases with depth when increasing the pulse moment. The combined kernel function shows significantly reduced sensitivity (Fig. 4 c, h), and therefore, these configurations cause significant NMR signal cancellation. For low ($q < 5$ As) pulse moments, the real part of the kernel function of the 35 m shifted configuration, i.e., placed outside the receiver loop, is different from those of the coincident loops, while the sensitivity becomes similar for higher pulse moments. As a result, the combined real part of the kernel function and the sounding curve derived for a fully saturated homogeneous ground do not cancel NMR signals for low q, while some cancellation is observed for higher q.

Second, to introduce an additional and therefore beneficial signal component, the reference loop is placed east of the coincident loop (Fig. 3 - blue dashed lines) to introduce a significant imaginary part to the kernel function (Fig. 5). While the real part exhibits only minor changes with respect to the case discussed above in which the reference is placed north, the imaginary part is changed and the overall detected signal amplitude is different when placing the reference loop eastwards (Fig. 5 e, j). Especially, the 35 m east-shifted non-remote receiver increases the amplitude of the synthetic sounding curve for almost all pulse moments, and the sensitivity to larger depths also remains due to the imaginary part.

Above, the position of the reference loop is evaluated. It is shown that a reference loop position outside and eastwards of the transmitter forces an imaginary part in the kernel function, which is beneficial. In the following, the loop size of the non-remote reference is investigated. Therefore, (i) a 5 m diameter loop is shifted again 35 m eastward and (ii) a 50 m diameter loop is shifted 50 m eastward (i.e., placed edge-to-edge) (Fig. 3 - gray dotted lines). It is shown (Fig. 6) that the 5 m configuration provides similar sensitivities and sounding curves as in the 10 m case, while the 50 m configuration is similar to the coincident loop alone. An interesting feature of the 5 m reference is the increase in the amplitudes of the sounding curve for pulse moments of approximately 3 As. This gain is due to a high sensitivity area in the imaginary part (Fig. 6b) close to the surface that is more prominent for the 5 m loop than for the 10 m loop.

In conclusion, the position and size of the non-remote reference significantly impacts the performance of the non-remote noise cancellation. It is found that using a 50 m transmitter loop with a 10 m reference loop placed a 35 m distance away from and east of the transmitter loop produces the best results within the tested set of locations and sizes. Nevertheless, further and detailed evaluation may discover even better configurations, and it is likely that a general scheme for different transmitter loop sizes can be developed. The sensitivity to the position and size of the reference loop illustrates that care must be taken to include these exact parameters in the kernel calculation. It is necessary to study the impact of positioning errors on the inversion result, which is beyond the scope of this paper. When using small loops, multiple turn loops are recommended to achieve a high signal amplitude above instrumental noise. Reducing the number of turns for small loops to increase the difference between the two kernel functions is compensated by the TF and thus makes no impact.

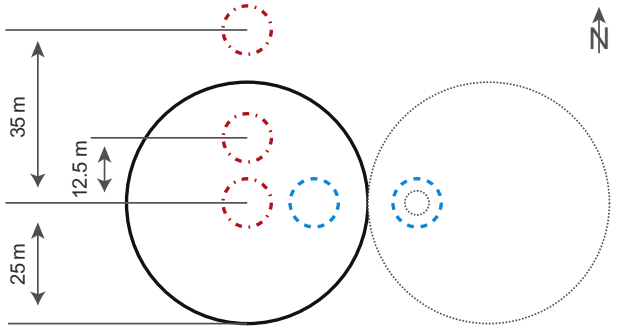

Fig. 3. Sketch of the reference loop sizes and positions. The black line indicates the 50 m coincident loop position. The red dotted-dashed lines indicate the reference loop positions used in Fig. 4, the blue dashed lines are the positions used in Fig. 5, and the gray dotted lines are the positions used in Fig. 6.

5.2. Complexity of the transfer function

In addition to the optimal position of the non-remote reference loop, the modification of $\mathbf{G_{Nx}}$ by the transfer function to achieve the final $\mathbf{G_{RNC}}$ (Eq. 19) is a critical part of the theoretical framework.

It is common to calculate the so-called local TFs (Müller-Petke and Costabel, 2014), i.e., correlate a single surface-NMR record with synchronously recorded single remote-reference loop data. This local TF is calculated for each record independently. This is possible because only the noise is correlated, and it therefore defines the correlation coefficient in the TF and ensures the most up-to-date TFs. Global TFs, on the other hand, are calculated using all records. Müller-Petke and Costabel (2014) show that local TFs typically exhibit superior performance compared with global TFs, as any variation in the noise with time causes a possible change in the TF with time and may impact the noise cancellation performance. If non-remote references are used, both the receiver and reference contain surface-NMR signals and thus cannot be used to calculate the TF. This results in the need to calculate the TF from noise records before or after each single surface-NMR experiment to obtain a local (but not perfectly up-to-date) TF or to use several noise records together to acquire the global TF. One may expect this approach to negatively impact non-remote reference noise cancellation. In contrast, one can also expect that the TF will generally be of lower complexity, i.e., showing less variation with time, due to the close proximity of the two loops.

Fig. 7 shows local TFs calculated from one-second-long records selected from a 30 s record and a global TF that uses the complete 30 s record. Both receiver loops are 10 m square loops. The data are again collected at the field site in Hannover, Germany. Because the site is in an urban environment, many different noise sources are present. The expectation of decreasing complexity with decreasing distance between the two recording loops is, at least for this field site, confirmed. While the TF correlation coefficients (both amplitude and phase) show significant variations with frequency if the loops are separated by 30 m and 50 m, the amplitude and phase of the TF for a separation of 10 m are almost constant. More importantly, due to the low complexity, the TF change with time is also low; consequently, one can expect that

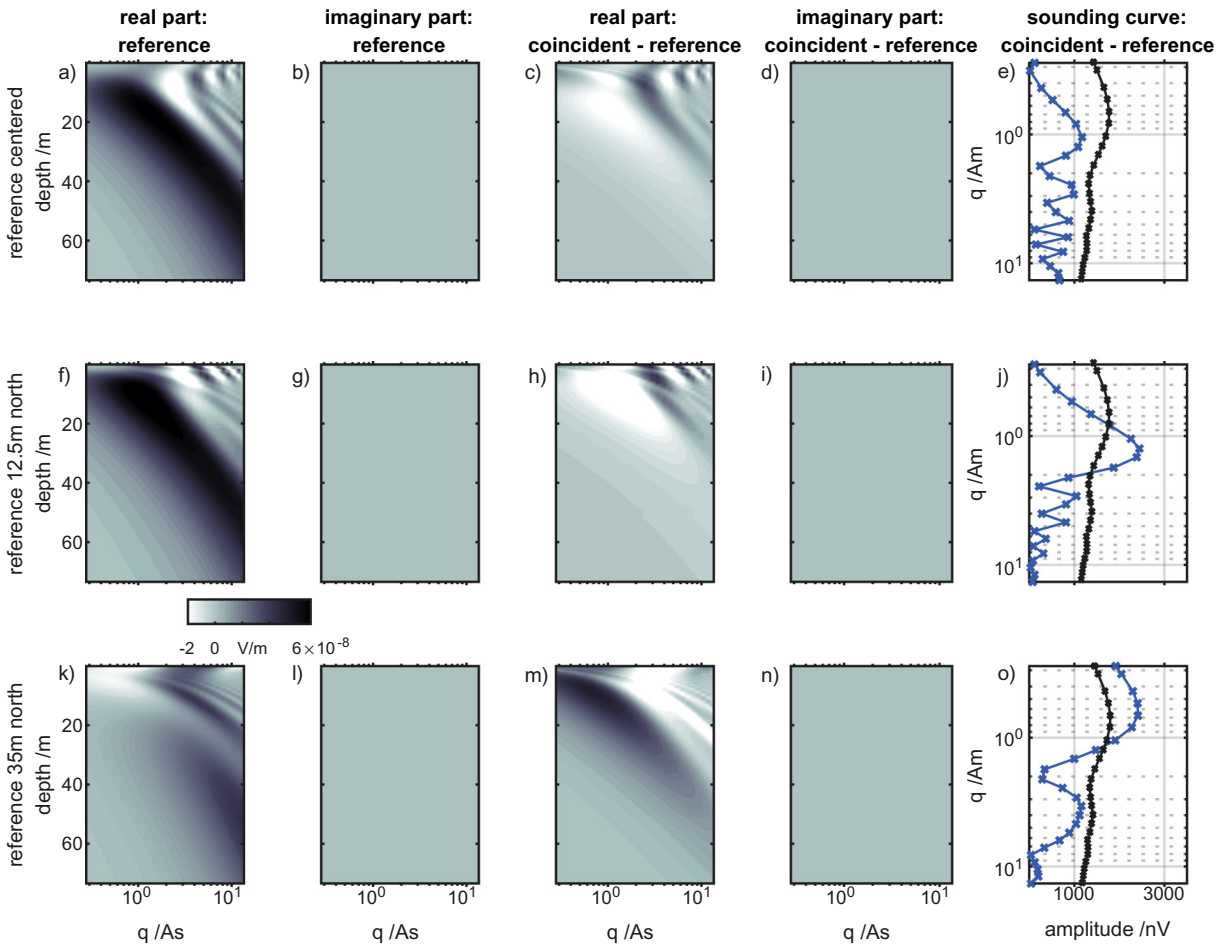

Fig. 4. Kernel functions (real and imaginary parts, first and second columns) of a separated 10 m diameter loop placed in the center, 12.5 m north and 35 m north of a 50 m diameter transmitter (see Fig. 3). Kernel function (real and imaginary parts, third and fourth columns) of the combined 50 m coincident loop and 10 m loop as a non-remote reference. The sounding curve for the combined setup (blue) is simulated for a fully saturated homogeneous ground. The coincident sounding is given as reference (black).

applying a global TF would not lead to reduced noise cancellation performance.

To further investigate this finding, Fig. 8 shows the time-domain signal before and after applying noise cancellation using both local and global TFs and two datasets with the loop distance varied. As expected, if the loops are close (10 m separation), there is almost no difference between local and global TFs (Fig. 8 b, c), and thus, the time variation of the TF can be neglected. The 50 m separation does exhibit differences, and the local TF provides a superior result (Fig. 8 e, f); thus, time variations are present and cannot be neglected. However, the final differences in the processed records are rather small, even though the differences in the TFs appear to be significant (Fig. 7 c, f). This example at least indicates that the disadvantage of non-remote references not using up-to-date noise, i.e., calculating the TF from records before or after the NMR experiment, is likely not very significant.

5.3. Semi-synthetic example

After studying the appropriate positioning of the reference loop and TFs separately, the remote reference and non-remote reference noise cancellation are compared with respect to a complete surface-NMR dataset. The loop layouts used are as follows: a 50 m circular loop as a transmitter and a receiver and (i) a 10 m circular loop placed 35 m east as a non-remote reference and (ii) a 10 m circular loop placed far away, i.e., in remote conditions. Layout (i) is the best non-remote layout found above. A synthetic 3-layer model that consists of an unsaturated layer (5% water content, 0.01 s relaxation time) down to 5 m, an aquifer (35% water content, 0.2 s relaxation time) down to 25 m and an aquitard (40% water content, 0.005 s relaxation time) is set up. Using this model, the forward response of a 50 m diameter circular loop is calculated (Fig. 9 a). The synthetic data are contaminated by the same two field noise datasets described in Fig. 8, i.e., one dataset with a 50 m separation between the two loops and the other with a 10 m separation. Each has two simultaneously recorded channels. The first channel of each noise dataset is used to contaminate the coincident loop data (Fig. 9 b, c). The second channel of the 50 m separation data is used to create a remote reference dataset. The second channel of the 10 m separation data is used to create a non-remote reference dataset. These surface-NMR data are calculated for a 10 m circular loop and a 35 m eastward-shifted separated loop. Note that all noise is scaled to the actual loop faces and that the surface-NMR signal is calculated as a 2103 Hz oscillation signal. Next, the dataset is processed identically to field data. This processing is independent and the same for the remote-reference and non-remote reference data. In both cases, global TFs are calculated, and the noise cancellation is applied. Further processing includes envelope detection and applying a low pass filter (500 Hz). Fig. 9 d and e shows the results. Clearly, both advantages of the non-remote approach are evident. The noise level is greatly reduced by a factor of 4 on average, and the signal amplitude is increased by a factor of 1.5 on average, leading to an overall increase in the signal-to-noise ratio of approximately 6.

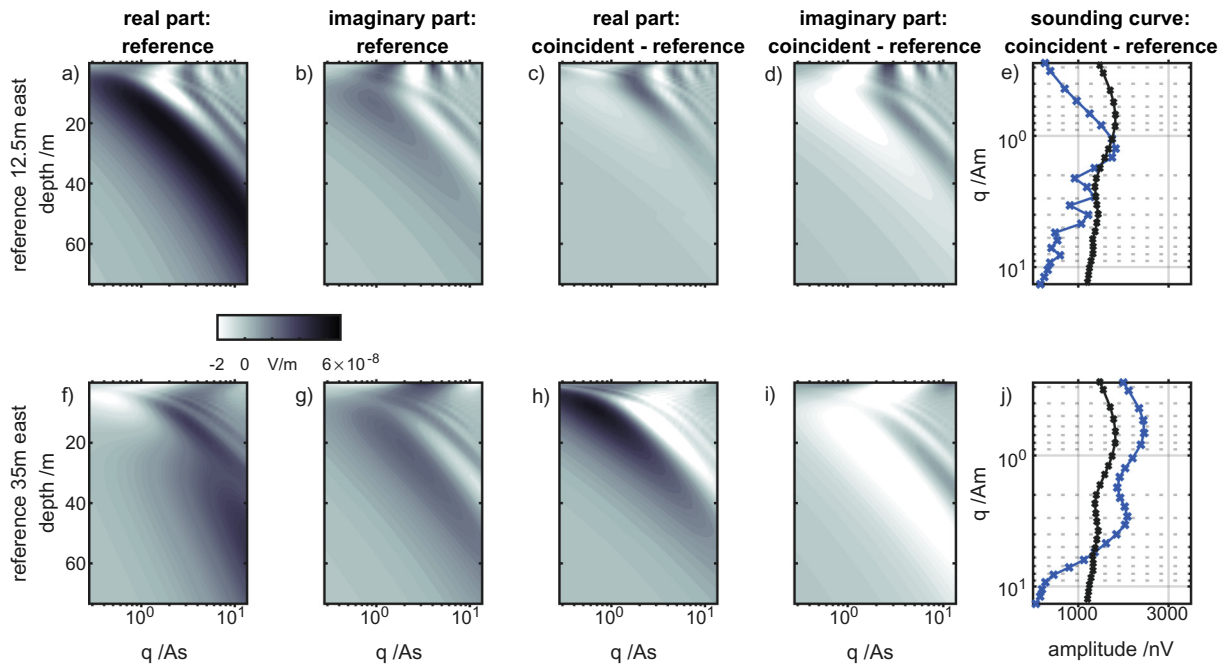

Fig. 5. Kernel functions (real and imaginary parts, first and second columns) of a separated 10 m diameter loop placed 12.5 m and 35 m east of a 50 m diameter transmitter (see Fig. 3). Kernel function (real and imaginary parts, third and fourth columns) of the combined 50 m coincident loop and a 10 m loop as a non-remote reference. The sounding curve for the combined setup (blue) is simulated for a fully saturated homogeneous ground. The coincident sounding is given as reference (black).

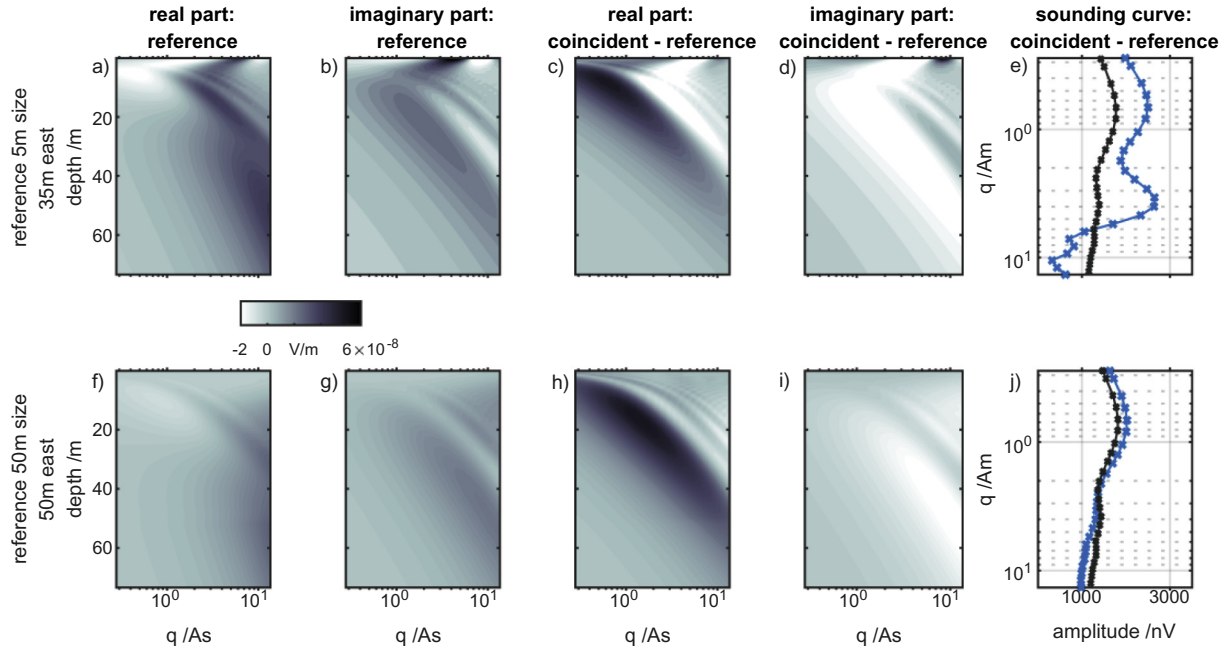

Fig. 6. Kernel functions (real and imaginary parts, first and second columns) of a separated 5 m diameter loop placed 35 m east and a 50 m diameter separated loop placed 50 m east of a 50 m diameter transmitter (see Fig. 3). Kernel function (real and imaginary parts, third and fourth columns) of the combined setup including the non-remote reference loop. The sounding curve for the combined setup (blue) is simulated for a fully saturated homogeneous ground. The coincident sounding is given as reference (black).

Finally, this semi-synthetic example allows for a numerical evaluation of the theoretical framework. The semi-synthetic data given in Fig. 9e are calculated using only well-tested algorithms and knowledge such as kernel calculation of coincident and separated loops, calculation of transfer functions from noise records and remote reference noise cancellation. All steps are performed independently. Using field noise, these data are as close as possible to field data. With an advantage over field data, the true model is perfectly known and allows for numerical confirmation of the developed approach. If the forward response of the combined kernel functions including the transfer function (Eq. 18)

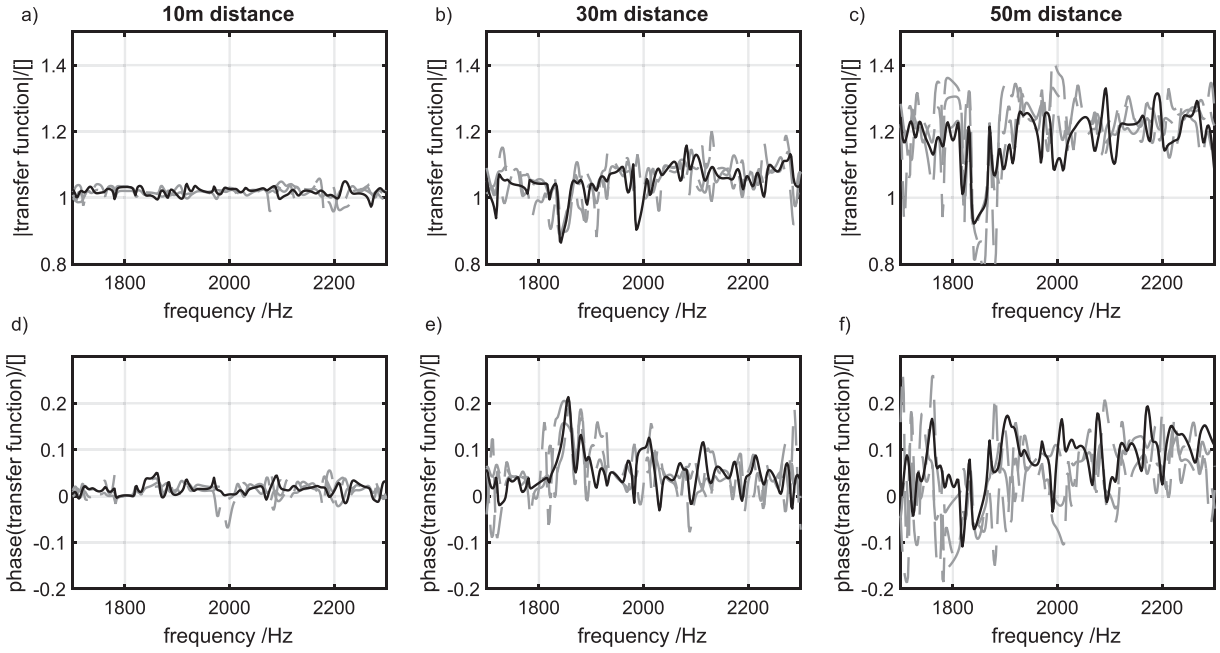

Fig. 7. Transfer function complexity (amplitude (a, b, c) and phase (d, e, f)) dependence on the distance and as a function of time. The reference loop is placed at distances from the detection loop of 10 m (a, d), 30 m (b, e) and 50 m (c, f). Transfer functions calculated from a continuous 30 s record using only one second (light gray lines) represent the local and with time changing trends, i.e., the local TF. The black lines show the transfer function calculated from the complete 30 s record representing the global trend, i.e., the global TF.

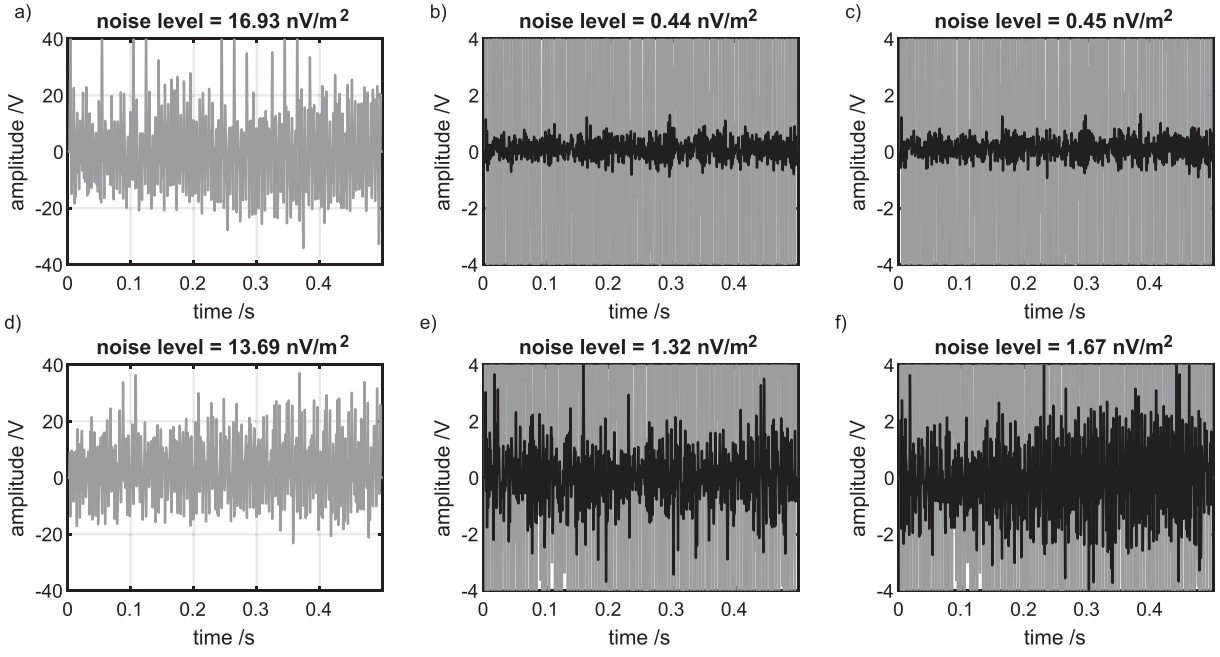

Fig. 8. NC performance for the records in a) and d) using the record itself to calculate the TF (b, e) or using the global transfer function calculated from 30 s records (c, f). The top panel (a, b, c) represents a 10 m distance between the transmitter and reference loops, and the bottom panel (d, e, f) represents a reference loop with a 50 m distance.

gives the same response as the semi-synthetic modeling above, then $\mathbf{G_{RNC}}$ is numerically confirmed and can be used for inversion. The results show (Fig. 10) that the obtained responses effectively coincide. Consequently, $\mathbf{G_{RNC}}$ can be used for inversion with no change to the commonly used inversion schemes. $\mathbf{G_{RNC}}$ does not change during the inversion, as the TF does not depend on the model. Thus, there are no additional non-linearities in the inversion. Additional uncertainties may arise if the TF is not adequately determined.

5.4. The figure-eight setup

Finally, the figure-eight approach is considered in the context of non-remote reference noise cancellation. In principle, the figure-eight approach is a sub-class of the non-remote references, with a figure-eight as a transmitter, two references positioned in an edge-to-edge configuration and a TF that equals 1. Fig. 11 shows the kernel function of an east-west oriented figure-eight with a 50 m loop size. It shows

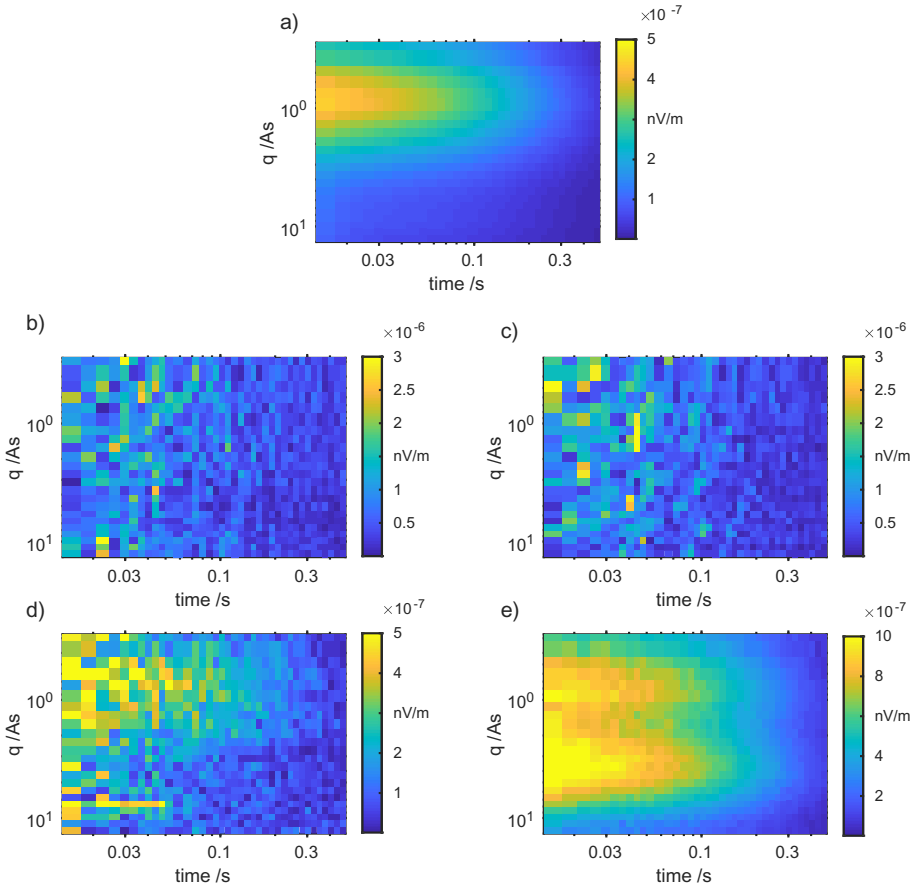

Fig. 9. Synthetic modeling study using real noise records. a) Forward response of a synthetic 3-layer model (described in the text) for a 50 m coincident loop. Noise contaminated dataset before (b) and after (d) remote noise cancellation. Noise contaminated dataset before (c) and after (e) non-remote noise cancellation. The non-remote reference loop is 10 m in size and placed 35 m east of the transmitter loop.

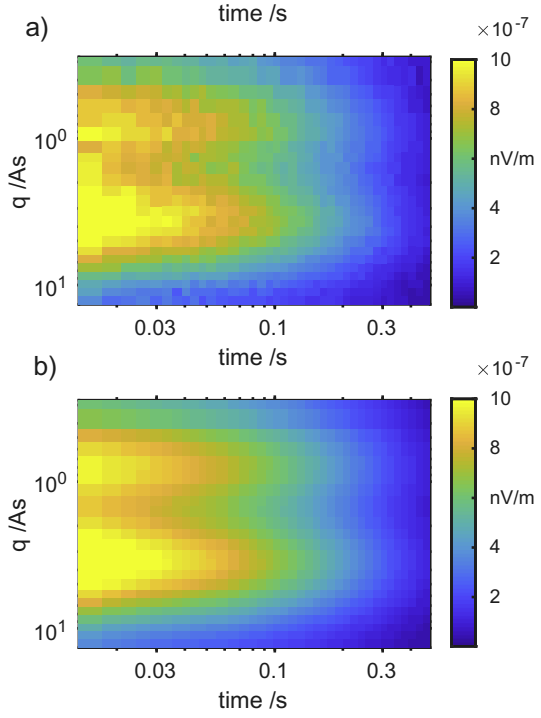

Fig. 10. Comparison of the data processing using a non-remote reference loop (Fig. 9e) and forward modeling based on eq. 18.

that the sounding curve and thus the detected signal amplitude are superior to all previously discussed non-remote layouts. However, there are disadvantages of the figure-eight that are closely interconnected. As the TF is basically 'hardwired', the layout must be perfectly oriented to provide optimal noise cancellation. This is time consuming and, in particular, not possible due to area limitations. Considering the time consumption, area limitation and 'hard-wired' TF, it may be advantageous to use figure-eights with unequal loop sizes and/or to record each receiver circle of the figure-eight independently and calculate a TF.

Using a pure noise dataset again, a 'hard-wired' figure-eight is compared with applying TF noise cancellation in which each circle is independently recorded in two channels (Fig. 12). Note that this figure-eight case is different from the above discussed edge-to-edge non-remote reference case, as here, the figure-eight is also transmitting. Furthermore, the orientations of the two loops are changed to the perpendicular direction to simulate a badly oriented figure-eight. The results show not only that the noise cancellation may be improved by applying a TF but also that the orientation of the figure-eight becomes less important.

6. Summary and conclusion

In this paper, the theoretical framework for using reference loops placed close to a transmitter loop is provided. The technique is referred to as non-remote reference noise cancellation (non-remote RNC). It is shown by field data that the performance, i.e., the ability to improve the SNR of surface-NMR measurements, depends on the distance between the detection and reference loops. The closer the reference loop

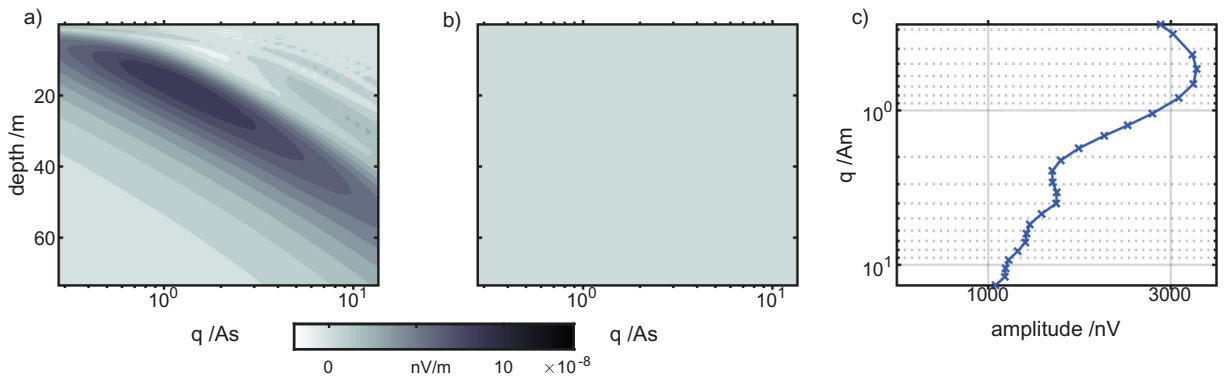

Fig. 11. Real part (a) and imaginary part (b) of a 50 m diameter east-west oriented figure-eight loop kernel function. The kernel function is calculated for a resistive subsurface and Earth's magnetic field of 48,000 nT with a 60 degrees inclination. The sounding curve (c) is simulated for a fully saturated homogeneous ground, i.e., it represents the maximum detectable signal amplitude.

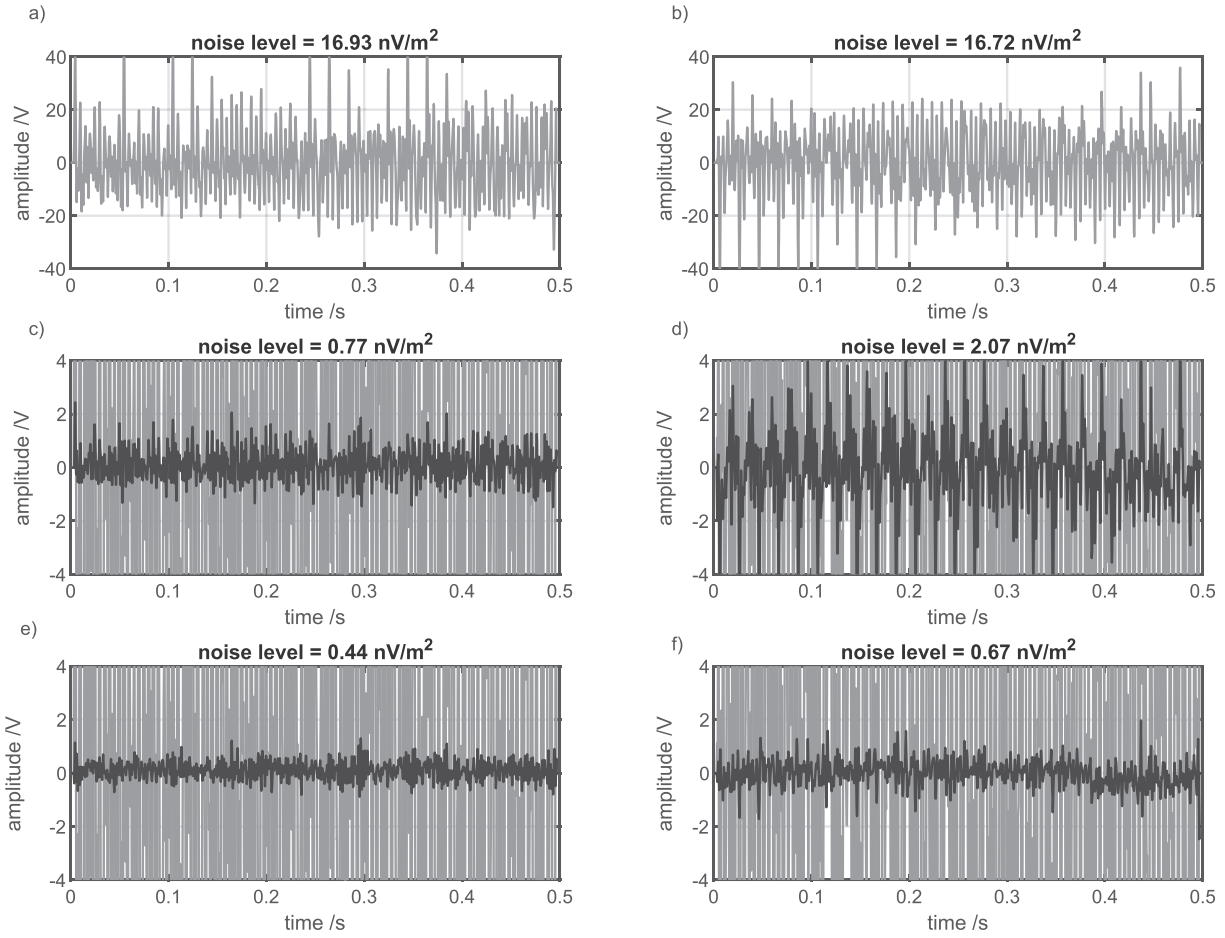

Fig. 12. Comparison of figure-eight-like signal subtraction and the use of non-remote reference transfer functions. Two figure-eight layout directions are investigated: east-west (a, c, e) and north-south (b, d, f). a) and b) show the records in one eastern (a) and southern (b) loop of the figure-eight setup. c) and d) show the result of the direct subtraction with the western (c) and northern (d) loops, i.e., simulating a common figure-eight measurement. e) and f) provide the resulting records when using a global transfer function instead of direct subtraction.

is to the detection loop, the lower the remaining electromagnetic noise after processing. It is demonstrated that the position and size of the reference loop cannot be chosen arbitrarily but must be carefully selected. It is found that using a 50 m transmitter loop and a 10 m reference loop placed within a 35 m distance east of the transmitter loop produces the best results within the tested set of locations and sizes. The approach can also be used with any existing measurements where a signal has been found in a reference given that the exact position and size of the reference are known. However, it should be kept in mind that the position and size of the loop substantially impact both the signal and it characteristics (real/imaginary parts). Some positions and sizes may cause larger signal attenuation than noise cancellation. It is further demonstrated that the often used figure-eight pattern, which needs to be carefully oriented to provide good noise cancellation properties, can be

improved by applying the concepts of non-remote RNC, i.e., handling the two detection parts of the figure-eight pattern independently.

Even though this paper provides evidence of the improved performance of non-remote RNC, a more general evaluation under several different field noise conditions must be carried out in the future. Further, a semi-synthetic example that uses only field noise but simulated surface-NMR data is presented. Both demands are beyond the scope of this paper, which is intended to demonstrate the general framework and feasibility of the concept. Finally, it is expected that the presented study of positioning of the reference loop reflects only a small subset of possibilities using the non-remote RNC approach.

Author statement

There is only a single author.

Declaration of Competing Interest

The authors declare that they have no known competing financial interests or personal relationships that could have appeared to influence the work reported in this paper.

Appendix A. Pseudo-code for non-remote NC

The following pseudo-code provides insight into how to handle non-remote noise cancellation in practice. In particular, code/functions are used as given in the Appendices in Müller-Petke et al. (2016).

```
%%%%%%%%%%%%%%%%%%%%%%%%%%%%%%%%%%%%%
% load the raw noise data (before envelope detection)
% of both loops and calculate the transfer function (TF);
% the noise data is recorded before the NMR experiment and
% used only to calculate the transfer function;
% loop 1: transmitter and detection loop -> n_rx
% loop 2: non-remote receiver loop -> n_nx
n_rx = load (' noiseDataLoop_1' );
n_nx = load(' noiseDataLoop_2' );
TF = FFTMultiChannelTransfer(n_rx,n_nx);

%%%%%%%%%%%%%%%%%%%%%%%%%%%%%%%%%%%%%
% load the raw data (before envelope detection).
% recorded during the NMR experiment.
% and apply the TF;
% t: time vector including dead time
% loop 1: transmitter and detection loop -> s
% loop 2: non-remote receiver loop -> r
s_raw = load(' DataLoop_1' );
r_raw = load(' DataLoop_2' );
% apply TF
s_raw_NC = s_raw - ifft(TF.*fft(r));
% calculate the envelope
s = SD(s_raw_NC,t)

%%%%%%%%%%%%%%%%%%%%%%%%%%%%%%%%%%%%%
% load field parameters (loop size, position, magnetic
field, ...);
% calculate the kernel functions;
% loop 1: transmitter and detection loop -> loop_1
% loop 2: non-remote receiver loop -> loop_2
loop_1 = load(' Loop_1_Parameters');
loop_2 = load(' Loop_2_Parameters');
g_Rx = calculateKernel(loop_1);
g_Nx = calculateKernel(loop_2);

%%%%%%%%%%%%%%%%%%%%%%%%%%%%%%%%%%%%%
% now we are ready for inversion
% here we give only a single step during the inversion
% for a full inversion this step is repeated until some
% stop criteria is reached
% T2: current T2 model
% w: current w model
% t: time vector including dead time

% prepare loop 1 kernel for QT
gM = repmat(g_s,length(t),1);
T2M = repmat(repmat(T2s.',size(g,1),1),length(t),1);
tM = kron(t,ones(size(g_s.'))).';
T2expM = exp(-tM./T2M);
G_Rx = gM.*T2expM;

% prepare loop 2 for QT
% compared to loop 1 the TF is included
gM = repmat(g_r,length(t),1);
T2M = repmat(repmat(T2s.',size(g,1),1),length(t),1);
tM = kron(t,ones(size(g_r.'))).';
% now we need to extend the QT envelope kernel temporarily
% to the original larmor-frequency (HF) apply the TF and
get back to the envelope signal
for iz=1:size(g_s,2)
for iq=1:size(g_s,1)
vec = size(g,1)*[ 0:1:length(t)-1] + iq;
% simulate a synthetic HF signal using the correct angles
of the kernel
HF = cos(2*pi*larmor.*t + angle(g_r(iq,iz)));
% apply the TF (that is in frequency domain)
% this is the key step: this includes the amplitude and
phase of the TF
% into the kernel of loop 2
HF_TF = ifft( TF .* fft(HF))
% get back to envelope
os(vec,iz) = SD(t, HF_TF);
end
end
T2expM = exp(-tM./T2M).*os;
G_Nx = gM.*T2expM;

% now we have both kernels and subtract
G_RNC = G_Rx - G_Nx;
% forward model the synthetic data for this step
D = G_RNC*w;
% difference to the measured data
dD = D - s;
% 'solve' for the model update,
% this includes several steps such as transformations and
line-search
dM = solve(dD, G, parameter)
```

References

Altobelli, S., Conradi, M.S., Fukushima, E., Hodgson, J., Nedwed, T., Palandro, D., Peach, A., Sowko, N., Thomann, H., 2019. Helicopter-borne. NMR for detection of oil under sea-ice. Marine Pollution Bulletin 144, 160–166.

Behroozmand, A.A., Auken, E., Fiandaca, G., Christiansen, A.V., 2012. Improvement in MRS parameter estimation by joint and laterally constrained inversion of MRS and TEM data. Geophysics 77, WB191–WB200.

Costabel, S., Günther, T., Dlugosch, R., Müller-Petke, M., 2016. Torus-nuclear magnetic resonance: Quasicontinuous airborne magnetic resonance profiling by using a helium-filled balloon. Geophysics 81, WB119–WB129.

Dalgaard, E., Auken, E., Larsen, J.J., 2012. Adaptive noise cancelling of multichannel magnetic resonance sounding signals. Geophys. J. Int. 191, 88–100.

Gamble, T.D., Goubau, W.M., Clarke, J., 1979. Magnetotellurics with a remote magnetic reference. Geophysics 44, 53–68.

Grombacher, D., Fiandaca, G., Auken, E., 2019. Estimating t2 from surface: NMR FID data using a forward model based on the full-bloch equation. Geophys. J. Int. 218, 1892–1902.

Grunewald, E., Grombacher, D., Walsh, D., 2016. Adiabatic pulses enhance surface nuclear magnetic resonance measurement and survey speed for groundwater investigations. Geophysics 81, WB85–WB96.

Hertrich, M., Braun, M., Yaramanci, U., 2005. Magnetic resonance soundings with separated transmitter and receiver loops. Near Surface Geophysics 3, 141–154.

Hertrich, M., Green, A.G., Braun, M., Yaramanci, U., 2009. High-resolution surface-NMR tomography of shallow aquifers based on multi-offset measurements. Geophysics 74, G47–G59.

Jiang, C., Müller-Petke, M., Lin, J., Yaramanci, U., 2015. Magnetic resonance tomography using elongated transmitter and in-loop receiver arrays for time-efficient 2-D imaging of subsurface aquifer structures. Geophys. J. Int. 200, 824–836.

Jiang, C., Müller-Petke, M., Wang, Q., Igel, J., 2018. Two-dimensional QT inversion of complex magnetic resonance tomography data. Geophysics 83, JM65–JM75.

Larsen, J.J., Dalgaard, E., Auken, E., 2014. Noise cancelling of MRS signals combining model-based removal of powerline harmonics and multichannel Wiener filtering. Geophys. J. Int. 196, 828–836.

Lehmann-Horn, J.A., Hertrich, M., Greenhalgh, S.A., Green, A.G., 2011. Three-dimensional magnetic field and NMR sensitivity computations incorporating conductivity anomalies and variable-surface topography. IEEE Transactions on Geoscience and Remote Sensing. 49, pp. 3878–3891.

Lin, T., Zhang, Y., Müller-Petke, M., 2019. Random noise suppression of magnetic resonance sounding oscillating signal by combining empirical mode decomposition and time-frequency peak filtering. IEEE Access 7, 79917–79926.

Liu, L., Grombacher, D., Auken, E., Larsen, J.J., 2019. Complex envelope retrieval for surface nuclear magnetic resonance data using spectral analysis. Geophys. J. Int. 217, 894–905.

Mueller-Petke, M., Yaramanci, U., 2010. QT inversion — Comprehensive use of the complete surface NMR data set. Geophysics 75, WA199–WA209.

Müller-Petke, M., Costabel, S., 2014. Comparison and optimal parameter setting of reference-based harmonic noise cancellation in time and frequency domain for surface-NMR. Near Surface Geophysics 12, 199–210.

Müller-Petke, M., Braun, M., Hertrich, M., Costabel, S., Walbrecker, J., 2016. MRSmatlab — a software tool for processing, modeling, and inversion of magnetic resonance sounding data. Geophysics 81, WB9–WB21.

Radic, T., 2006. Improving the signal-to-noise ratio of surface NMR Data due to the remote reference technique: near surface 2006. 12th European meeting of Environmental and Engineering Geophysics, Helsinki, Finland, 4-6th September, pp. 1–4.

Skibbe, N., Günther, T., Müller-Petke, M., 2018. Structurally coupled cooperative inversion of magnetic resonance with resistivity soundings. Geophysics 83, JM51–JM63.

Trushkin, D.V., Shushakov, O.A., Legchenko, A.V., 1994. The potential of a noise-reducing antenna for surface NMR groundwater surveys in the earth's magnetic field. Geophysical Prospecting 42, 855–862.

Walsh, D.O., 2008. Multi-channel surface NMR instrumentation and software for 1D/2D groundwater investigations. J. Appl. Geophys. 66, 140–150.

Wang, Q., Jiang, C., Müller-Petke, M., 2018. An alternative approach to handling co-frequency harmonics in surface nuclear magnetic resonance data. Geophys. J. Int. 215, 1962–1973.